INSTITUTE OF PHYSICS PUBLISHING MODELLING AND SIMULATION IN MATERIALS SCIENCE AND ENGINEERING

Modelling Simul. Mater. Sci. Eng. **13** (2005) 733–751 doi:10.1088/0965-0393/13/5/007

Mesoscale simulation of the kinetics and topology of spherulite growth during crystallization of isotactic polypropylene (iPP) by using a cellular automaton

D Raabe[1] **and A Godara**

Max-Planck-Institut für Eisenforschung, Max-Planck-Str. 1, 40237 Düsseldorf, Germany

E-mail: raabe@mpie.de

Received 8 October 2004, in final form 29 April 2005
Published 24 June 2005
Online at stacks.iop.org/MSMSE/13/733

Abstract

The kinetics and topology of spherulite growth during crystallization of isotactic polypropylene (iPP) has been studied by using a three-dimensional cellular automaton model. The automaton cells can assume one out of two discrete states, i.e. *melt* or *spherulite*. The transformation kinetics governing the individual cell switches from *melt* to *spherulite* is formulated according to the Hoffman–Lauritzen secondary surface nucleation and growth theory for spherulite expansion. It is used to calculate the switching probability of each cell as a function of its previous state and the state of the neighbour cells. The actual switching decision is made by evaluating the Hoffman–Lauritzen switching probability calculated locally by using a Monte Carlo step. The growth rule is scaled by the ratio of the local and maximum occurring Gibbs free energy of transformation, the local and maximum occurring temperature and by the size of the automaton cells. The Hoffman–Lauritzen scaling procedure provides a real time and a real space scale. The simulations are conducted for quiescent and for weakly sheared melts. The kinetics predicted are in excellent agreement with those obtained for iPP from experiments.

1. Introduction to the modelling of spherulite growth kinetics in polymers

Quantitative mesoscale kinetic simulations of structure and topology evolution during polymer solidification is an important issue in the field of advanced polymer processing [1–7]. Among the various structural phenomena involved, crystallization plays a major role in that context. In the field of polymer solidification, mesoscopical simulation methods which are discrete in space and time are particularly valuable since spherulite growth during crystallization occurs mostly under inhomogeneous mechanical and thermal boundary conditions.

[1] Author to whom any correspondence should be addressed.

Earlier approaches to the modelling of crystallization processes in polymers were suggested and discussed in detail by various groups. For instance, Koscher and Fulchiron [1] studied the influence of shear on polypropylene crystallization experimentally, and also in terms of a kinetic model for crystallization under quiescent conditions and under the influence of shear. Their approach was based on a classical topological Avrami–Johnson–Mehl–Kolmogorov (AJMK) model for isothermal conditions and on related statistical models such as those of Nakamura *et al* [6] and Ozawa [7] for non-isothermal conditions. The authors found in part excellent agreement between these modelling results and their own experimental data. For predicting crystallization kinetics under *shear* conditions, Koscher and Fulchiron [1] used an AJMK model in conjunction with a formulation for the additional number of shear-induced nuclei. They related the increase in the density of nuclei to the first normal stress difference. The authors justified this approach by suggesting that the first normal stress difference includes the effects of the elastic portion of the rheological behaviour of the material. They assumed that the systematic shear and alignment of certain preferred molecular orientations may predispose and, thereby, favour oriented clustering of molecular segments initiating additional nucleation [8]. The latter part of the approach was based on an earlier study of Eder *et al* [9, 10] who expressed the number of activated nuclei as a function of the square of the shear rate which provides the possibility of predicting the thickness of thread-like precursors. A related approach was published by Hieber [11] who used the Nakamura equation [6] to establish a direct relation between the Avrami and the Ozawa [7] crystallization rate constants.

AJMK-based transformation models have been applied to polymers with great success in cases where the underlying assumption of material homogeneity is reasonably fulfilled [1–11]. It is, however, likely that further progress in understanding and tailoring polymer microstructures can be made by the use of cellular automata [12–20]. These approaches are designed to cope with more realistic situations in terms of the heterogeneity of the material and of the boundary conditions encountered.

The aim of our study, therefore, is to use a three-dimensional probabilistic cellular automaton model for the prediction of the kinetics and topology of spherulite growth during crystallization of isotactic polypropylene (iPP) [12]. The model uses experimental and theoretical input parameters which were adopted together with the corresponding experimental data on the topology and kinetics of iPP from the literature [1] and also directly from the group of Fulchiron [21].

2. The cellular automaton model for polymer spherulite growth

2.1. Structure of the automaton model

The model for the mesoscale prediction of spherulite growth in partially crystalline polymers is formulated as a three-dimensional cellular automaton with a probabilistic transition rule [12, 16–20]. It is discrete in time and real space. It uses a cubic lattice and considers the states of the three nearest neighbour shells for the calculation of cell switches. The equivalent real-time kinetics of the cell switches is scaled on the basis of the Hoffman–Lauritzen rate theory for spherulite growth. This formulation is used to calculate the local transformation kinetics in terms of the switching probability of each cell, as a function of its earlier state and the state of the neighbouring cells.

The thermodynamic driving force for cell flips is the (scalar) Gibbs free energy G_t per switched cell associated with the transformation between the quiescent or weakly sheared melt and the partially crystalline solid. Configurational (capillary) thermodynamic

driving forces are not taken into account owing to the very small interface energy in such systems, i.e. curvature-driven coarsening does not take place in the simulation (and, by practical means, not in experiments either). The low value of the interface energy between an expanding spherulite and its disordered melt environment is due to the fact that the spherulite itself is not fully crystalline but is a two-phase aggregate consisting of heavily branched crystalline lamellae with considerable portions of amorphous chains between them. Hence only a small part of the actual interface between such a semi-crystalline spherulite and the melt provides a contribution to the interface energy (crystal-melt) while others (liquid melt–solid melt) do not do so.

The actual decision with regard to a state flip event is made by evaluating the analytically calculated local switching probability via a Monte Carlo step. The growth rule is scaled by the ratio of the local and the maximum possible interface properties, the local and maximum occurring Gibbs free energy of transformation, the local and maximum occurring temperature and by the spacing of the grid points (cell size). The use of experimental input data for iPP from the literature [1] and from the group of Fulchiron [21] (see details later) allows us to make predictions on a real time and space scale. The transformation rule is scalable to any mesh size and to any spectrum of interface and transformation data. The state update of all grid points is made in synchrony, as in all automata [12–20]. In order to avoid confusion with the Potts model or related Ising-type approximations, one should stress that except for the probabilistic evaluation of the analytically calculated transformation probabilities, the current automaton approach is entirely deterministic. Artificial thermal fluctuation terms, other than those principally included through the Boltzmann factors, are not permitted.

Independent variables of the automaton are time t and space $\boldsymbol{x} = (x_1, x_2, x_3)$ (bold symbols refer to vector quantities). Space is discretized into an array of cubic cells. The state of each cell is characterized in terms of the dependent field variables which are, the temperature field, the phase state (*melt* or partially crystalline *spherulite*) and the transformation and interface energies.

The starting data, i.e. the spatial map of the melt (which corresponds to the spatial distribution of the Gibbs free energy of the transformation) and of the temperature field must be provided by experiment or theory. In this study, we assume a homogeneous distribution of the melt properties in order to compare the predictions with experimental data for quiescent or nearly quiescent melt conditions.

The overall kinetics of the automaton result from the collective evolution of all cell switches. Each cell flip occurs in accordance with a switching rule which determines the individual switching probability of each cell as a function of its previous state, and the state of the neighbouring cells. The switching rule used in this study is designed for the simulation of static crystallization of a quiescent or weakly sheared supercooled amorphous melt [12]. It shows that the state of a non-crystallized cell belonging to an amorphous region (which is in state *melt*) may change owing to the expansion of a crystallizing neighbouring spherulite (which is in state *spherulite*) which grows according to the local temperature, Gibbs free energy associated with that transformation and interface properties. If such an expanding spherulite sweeps a non-crystallized cell the energy of that cell changes and from there on is attributed to the expanding neighbouring spherulite. The scaling procedure which assigns a real time scale to these individual cell switches is outlined in the ensuing sections.

2.2. Rate equation for polymer spherulite growth

Since the 1950s it has been known that many polymers form chainfolded lamellar crystals from a solution or melt [22–26]. Most theories of polymer crystallization date back to the

studies of Turnbull and Fisher [27], where the rate of nucleation is formulated in terms of two Boltzmann expressions quantifying the transport across the interface and the free enthalpy barrier associated with the critical nucleus.

On the basis of this early work [27], Hoffman and Lauritzen [22] developed a more detailed rate equation for polymer spherulite growth in which the rate of nucleation is formulated in terms of the product of two Boltzmann expressions, one quantifying the expansion of the growth interface in terms of the activation energy required for further molecule or block alignment steps, and the other involving the energy for secondary nucleation on existing crystalline lamellae. Overviews on spherulite growth kinetics were given by Hoffman *et al* [23], Hoffman and Miller [24], Keller [28], Snyder *et al* [29,30] and Long *et al* [31].

The rate equation by Hoffman and Lauritzen is used as a basis for the formulation of the switching rule of the cellular automaton model used in this study [12]. It describes interface motion in terms of lateral and forward molecule or, alternately, block precursor alignment and disalignment processes at a homogeneous planar portion of an interface segment between a semi-crystalline spherulite and the melt. It is important to note that the Hoffman and Lauritzen rate theory is a coarse-grained formulation which homogenizes over two rather independent sets of very anisotropic mechanisms, namely, secondary nucleation on the lateral surface of the growing lamellae (creating strong lateral, i.e. out-of-plane volume expansion and new crystallographic orientations) and lamella growth (creating essentially two-dimensional, i.e. in-plane expansion and crystallographic orientation continuation). Although the two basic ingredients of this rate formulation are individually of a highly anisotropic character, the overall spherulite equation assumes an isotropic form. This net shape isotropy arises from the fact, that although the crystalline portions evolve individually in an anisotropic way, the residual melt is frozen in between the crystalline lamellae, rendering the overall shape isotropic.

The basic rate equation is

$$\dot{\boldsymbol{x}} = \dot{\boldsymbol{x}}_{\mathrm{p}} \exp\left(-\frac{Q^*}{R\,(T - T_\infty)}\right) \exp\left(-\frac{K_{\mathrm{g}}}{T\,\Delta T}\right), \tag{1}$$

where $\dot{\boldsymbol{x}}$ is the velocity vector of the interface between the spherulite and the supercooled melt, $\dot{\boldsymbol{x}}_{\mathrm{p}}$ is the pre-exponential velocity vector, ΔT is the supercooling defined by $\Delta T = T_{\mathrm{m}}^0 - T$, where T_{m}^0 is the equilibrium melting point (valid for a very large crystal formed from fully extended chains, i.e. no effects of free surfaces are included), Q^* is the activation energy for viscous molecule flow or, alternately, attachment of the chain or crystalline block to the crystalline surface, T_∞ is the temperature below which all viscous flow stops (glass transition temperature; temperature at which the viscosity exceeds the value of $10^{13}\,\mathrm{N\,s\,m^{-2}}$), K_{g} the secondary nucleation exponent and T the absolute temperature.

According to Hoffman and co-workers [22–24] the exponent K_{g} amounts to

$$K_{\mathrm{g}} = \frac{\xi b \sigma \sigma_{\mathrm{e}} T_{\mathrm{m}}^0}{k_{\mathrm{B}} \Delta G_{\mathrm{f}}}, \tag{2}$$

where k_{B} is the Boltzmann constant, ξ, a constant which equals 4 for growth regimes I and III, and 2 for growth regime II [24,32], b is the thickness of a crystalline lattice cell in the direction of growth, σ is the free energy per area for the interface between the lateral surface and the supercooled melt σ_{e} is the free energy per area for the interface between the fold surface where the molecule chains fold back or emerge from the lamella and the supercooled melt and ΔG_{f} is the Gibbs free energy of fusion at the crystallization temperature which is approximated by $\Delta G_{\mathrm{f}} \approx (\Delta H_{\mathrm{f}} \Delta T)/T_{\mathrm{m}}$.

The different growth regimes, I (shallow quench regime), II (deep quench regime) and III (very deep quench regime) were discussed by Hoffman and Miller [24] such that, within regime I, the spherulite expansion is governed by weak secondary nucleation and preferred forward lamellae growth. Nucleation is, in this regime, dominated by the formation of few single surface nuclei which are referred to as stems. It is assumed that when one stem is nucleated, the entire new layer is almost instantaneously completed relative to the nucleation rate. In regime II, the two rates are comparable and is the normal condition for spherulitic growth having a weaker ΔT dependence than regime I. Regime III is characterized by the nucleation of many nuclei entailing disordered crystal growth. Nucleation is, in this regime, more important than growth.

According to [24], the pre-exponential velocity vector for an interface between a spherulite and the melt can be modelled according to

$$\dot{\boldsymbol{x}}_{\mathrm{p}} = \boldsymbol{n}\frac{N_0 b J}{\ell_u}\left[\frac{k_{\mathrm{B}}T}{b\sigma} - \frac{k_{\mathrm{B}}T}{2b\sigma + ab\Delta G_{\mathrm{f}}}\right], \tag{3}$$

where N_0 is the number of initial stems, $\boldsymbol{n}$ the unit normal vector of the respective interface segment and ℓ_u the monomer length. J amounts to

$$J = \frac{\varsigma}{n_z}\left(\frac{k_{\mathrm{B}}T}{h}\right), \tag{4}$$

where ς is a constant for the molecular friction experienced by the chain as it is reeled onto the growth interface, n_z the number of molecular repeat units in the chain and h the Planck constant. The fraction $k_{\mathrm{B}}T/h$ amounts to a frequency pre-factor. These terms yield a Hoffman–Lauritzen–Miller type version [24] of a velocity-rate vector equation for spherulite growth under consideration of secondary nucleation:

$$\dot{\boldsymbol{x}} = \boldsymbol{n}\frac{N_0 b\varsigma}{\ell_u n_z}\left(\frac{k_{\mathrm{B}}T}{h}\right)\left[\frac{k_{\mathrm{B}}T}{b\sigma} - \frac{k_{\mathrm{B}}T}{2b\sigma + ab\Delta G_{\mathrm{f}}}\right]\exp\left(-\frac{Q^*}{R\,(T - T_\infty)}\right)\exp\left(-\frac{\xi b\sigma\sigma_{\mathrm{e}}T_{\mathrm{m}}^0}{k_{\mathrm{B}}T\,\Delta T\,\Delta G_{\mathrm{f}}}\right). \tag{5}$$

2.3. Mapping the rate equation on a cellular automaton mesh

For dealing with competing flip events (attempted by different neighbouring sites) which may address one and the same lattice cell in an automaton, the statistical rate equation can be formulated as a probabilistic analogue which allows one to calculate switching *probabilities* for the states of the automaton cells [16, 17]. For this purpose, the rate formulation (equation (5)) is separated into a non-Boltzmann part, $\dot{\boldsymbol{x}}_0$, which has a weak temperature dependence, and a Boltzmann part, w, which depends exponentially on temperature, with

$$\dot{\boldsymbol{x}}_0 = \boldsymbol{n}\frac{N_0 b\varsigma}{\ell_u n_z}\left(\frac{k_{\mathrm{B}}T}{h}\right)\left[\frac{k_{\mathrm{B}}T}{b\sigma} - \frac{k_{\mathrm{B}}T}{2b\sigma + ab\Delta G_{\mathrm{f}}}\right], \qquad \dot{\boldsymbol{x}} = \dot{\boldsymbol{x}}_0 w$$
$$\text{and} \quad w = \exp\left(-\frac{Q^*}{R\,(T - T_\infty)}\right)\exp\left(-\frac{\xi b\sigma\,\sigma_{\mathrm{e}}T_{\mathrm{m}}^0}{k_{\mathrm{B}}T\,\Delta T\,\Delta G_{\mathrm{f}}}\right). \tag{6}$$

The Boltzmann factors in w represent the probability for cell flips. According to this equation, non-vanishing switching probabilities occur for pairs of cells with different temperatures and/or transformation energies. The automaton considers the first, second (two-dimensional) and third (three-dimensional) neighbouring shell for the calculation of the switching probability acting on a cell.

2.4. Scaling procedure

Cellular automata are commonly applied to matrix data which have a spatial resolution above the molecular scale. This means that the automaton grid has a cell size $\lambda_m \gg b$ (where b is the thickness of a crystalline lattice cell in the spherulite). If a moving boundary segment sweeps a cell, the spherulite thus grows (or shrinks) by λ_m^3 rather than b^3. Since the net velocity of an interface segment (between a partially crystalline spherulite and the melt) must be independent of the imposed value of λ_m, an increase in jump width must entail a corresponding drop in the grid attack frequency, i.e. an increase of the characteristic time step and vice versa. For obtaining such a scale-independent formulation for the interface velocity, the grid frequency must be chosen in a way that ensures that the attempted switch of a cell of length λ_m occurs with a frequency much below the molecular attack frequency (which would be of the order of the Debye frequency), which attempts to switch a cell of length b. Mapping the rate equation on such an imposed grid which is characterized by an external scaling length (lattice parameter of the mesh) λ_m leads to the equation

$$\dot{\boldsymbol{x}} = \dot{\boldsymbol{x}}_0 w = \boldsymbol{n}(\lambda_m \nu) w \qquad \text{with } \nu = \frac{N_0 b \varsigma}{\lambda_m \ell_u n_z} \left(\frac{k_B T}{h}\right) \left[\frac{k_B T}{b\sigma} - \frac{k_B T}{2b\sigma + ab\Delta G_f}\right], \tag{7}$$

where ν is the eigenfrequency of the automaton grid which is characterized by the magnitude of λ_m.

2.5. Normalization of the switching probability

The eigenfrequency given by equation (7) represents the attack frequency which is valid for *one* interface segment with constant properties moving in a constant temperature field. In order to include a larger spectrum of possible interface properties (e.g. due to temperature gradients) in one simulation, it is necessary to normalize equation (7) by a general grid attack frequency ν_0 which is *common* to all interfaces in the system, i.e.

$$\dot{\boldsymbol{x}} = \dot{\boldsymbol{x}}_0 w = \boldsymbol{n} \lambda_m \nu_0 \left(\frac{\nu}{\nu_0}\right) w = \hat{\dot{\boldsymbol{x}}}_0 \left(\frac{\nu}{\nu_0}\right) w = \hat{\dot{\boldsymbol{x}}}_0 \hat{w}, \tag{8}$$

where the normalized switching probability amounts to

$$\begin{aligned} \hat{w} = \left(\frac{\nu}{\nu_0}\right) \exp\left(-\frac{Q^*}{R\,(T - T_\infty)}\right) \exp\left(-\frac{\xi b\sigma \sigma_e T_m^0}{k_B T \Delta T \Delta G_f}\right) = \frac{N_0 b \varsigma}{\nu_0 \lambda_m \ell_u n_z} \left(\frac{k_B T}{h}\right) \\ \times \left[\frac{k_B T}{b\sigma} - \frac{k_B T}{2b\sigma + ab\Delta G_f}\right] \exp\left(-\frac{Q^*}{R\,(T - T_\infty)}\right) \exp\left(-\frac{\xi b\sigma \sigma_e T_m^0}{k_B T \Delta T \Delta G_f}\right). \end{aligned} \tag{9}$$

The value of the normalization or grid attack frequency ν_0 can be identified by using the plausible assumption, that the maximum occurring switching probability cannot assume a state above one.

$$\begin{aligned} \hat{w}^{\max} = \frac{N_0 b \varsigma}{\nu_0 \lambda_m \ell_u n_z} \left(\frac{k_B T_{\max}}{h}\right) \left[\frac{k_B T_{\max}}{b\sigma_{\min}} - \frac{k_B T_{\max}}{2b\sigma_{\min} + ab\Delta G_f}\right] \\ \times \exp\left(-\frac{Q^*}{R\,(T_{\max} - T_\infty)}\right) \exp\left(-\frac{\xi b\sigma_{\min} \sigma_{e,\min} T_m^0}{k_B T_{\max} \Delta T_{\max} \Delta G_{f,\max}}\right) \overset{!}{\leqslant} 1, \end{aligned} \tag{10}$$

where $T_{\max}$ is the maximum occurring temperature in the system, $\Delta T_{\max}$ the maximum occurring supercooling, $\sigma_{\min}$ the minimum occurring lateral interface energy (for instance, in cases where a crystallographic orientation dependence of the interface energy exists),

$\Delta G_{\mathrm{f,max}}$ the maximum Gibbs free transformation energy which depends on the local temperature, i.e. $\Delta G_{\mathrm{f,max}} \approx (\Delta H \Delta T_{\max})/T_{\mathrm{m}}^{0}$ and $\sigma_{\mathrm{e,min}}$ the minimum occurring fold interface energy. For $\hat{w}^{\max} = 1$, one obtains the normalization frequency $\nu_0^{\min}$, as a function of the upper-bound input data.

$$\nu_0^{\min} = \frac{N_0 b \varsigma}{\lambda_{\mathrm{m}} \ell_u n_z} \left(\frac{k_{\mathrm{B}} T_{\max}}{h}\right) \left[\frac{k_{\mathrm{B}} T_{\max}}{b\sigma_{\min}} - \frac{k_{\mathrm{B}} T_{\max}}{2b\sigma_{\min} + ab\Delta G_{\mathrm{f}}}\right] \times \exp\left(-\frac{Q^*}{R\,(T_{\max} - T_\infty)}\right) \exp\left(-\frac{\xi b \sigma_{\min} \sigma_{\mathrm{e,min}} T_{\mathrm{m}}^{0}}{k_{\mathrm{B}} T_{\max} \Delta T_{\max} \Delta G_{\mathrm{f,max}}}\right). \tag{11}$$

This frequency must be calculated only once per simulation and it normalizes all other switching processes. The insertion of this basic attack frequency of the grid into equation (9) yields an expression for calculating the local values of the switching probability as a function of temperature and energy:

$$\hat{w}^{\mathrm{local}} = \left(\frac{T_{\mathrm{local}}}{T_{\max}}\right) \frac{[(k_{\mathrm{B}} T_{\mathrm{local}}/b\sigma_{\mathrm{local}}) - (k_{\mathrm{B}} T_{\mathrm{local}})/(2b\sigma_{\mathrm{local}} + ab\Delta G_{\mathrm{f,local}})]}{[(k_{\mathrm{B}} T_{\max}/b\sigma_{\min}) - (k_{\mathrm{B}} T_{\max})/(2b\sigma_{\min} + ab\Delta G_{\mathrm{f,max}})]} \times \exp\left(-\left[\left(\frac{Q^*}{R}\right)\left(\frac{1}{T_{\mathrm{local}} - T_\infty} - \frac{1}{T_{\max} - T_\infty}\right)\right]\right) \times \exp\left(-\left[\left(\frac{\xi b T_{\mathrm{m}}^{0}}{k_{\mathrm{B}}}\right)\left(\frac{\sigma_{\mathrm{local}}\sigma_{\mathrm{e,local}}}{T_{\mathrm{local}} \Delta T_{\mathrm{local}} \Delta G_{\mathrm{f,local}}} - \frac{\sigma_{\min}\sigma_{\mathrm{e,min}}}{T_{\max} \Delta T_{\max} \Delta G_{\mathrm{f,max}}}\right)\right]\right). \tag{12}$$

This expression is the central switching equation of the algorithm. For isothermal crystallization conditions, the expression becomes simpler since the local temperature is the same as the global temperature, i.e. $T_{\max}$ is identical to T_{local}, and the maximum occurring supercooling is the same as the global supercooling, i.e. $\Delta T_{\max}$ is identical to $\Delta T_{\mathrm{local}}$.

The cellular automaton generally works in such a way that an existing (expanding) spherulite *infects* its neighbour cells at a rate or, alternately, with a probability which is determined by equation (12). Hence wherever a partially crystalline spherulite has the topological possibility of expanding into a neighbouring cell which is in state *melt*, the automaton rule uses equation (12) to quantify the probability of that cell switch using the local state variable data which characterize the two neighbouring cells. Equation (12) shows that local switching probabilities derived by rate theory can be quantified in terms of the ratio of the local and the maximum temperature and the corresponding ratio of the interface properties. The probability of the fastest occurring interface segment to realize a cell switch is equal to 1. The equation also shows that the mesh size of the automaton does not influence the switching probability, but only the time step elapsing during an attempted state flip. The characteristic time constant of the simulation Δt, amounts to $1/\nu_0^{\min}$.

2.6. The switching decision

In the current automaton formulation, competing switches (from different neighbours) which aim at flipping the state of the same cell are evaluated by stochastic sampling. For this purpose, equation (12) is at first used to calculate the *probability,* $\hat{w}_{\mathrm{local}}$, of all competing cell flips. The actual *decision* about the success of a switch is then made by a Monte Carlo step. The use of random sampling ensures that all cells have a chance to switch according to their correct statistical weight. Hence for each cell, the calculated switching probability is compared to a randomly generated number r which lies between 0 and 1. The switch is accepted if the

random number is equal to or smaller than the calculated switching probability; otherwise the switch is rejected.

$$\text{Random number } r \text{ between 0 and 1} \begin{cases} \text{accept switch,} & \text{if} \quad r \leqslant \hat{w}^{\text{local}}, \\ \text{reject switch,} & \text{if} \quad r > \hat{w}^{\text{local}}. \end{cases} \tag{13}$$

Except for the probabilistic evaluation of the analytically calculated transformation probabilities, the approach is entirely deterministic. Artificial thermal fluctuation terms other than those principally included through the Boltzmann factors are not permitted. The use of realistic or even experimental input data for the interface energies and transformation enthalpies enables one to introduce scale. The switching rule is scalable to any mesh size and to any spectrum of interface energy and Gibbs free transformation energy data. The state update of all cells is made in synchrony, as in all automata.

2.7. Scaling procedure on the basis of data for iPP

Time and length scaling of the system enters through the physical parameters which characterize the polymer under investigation, and through the mesh parameter of the automaton. The central scaling expression is given by equation (11) in conjunction with the terms given by equations (2)–(5). The inverse of the frequency given by equation (11) is the basic time step of the simulation, during which each cell makes one attempt to flip in accordance with its individual local switching probability (equation (13)). The current simulations use material data for iPP taken from [1] and from the group of Fulchiron [21]. The material has a molecular weight of $M_{\text{w}} = 180.3 \times 10^3 \,\text{g mol}^{-1}$ and a polydispersity index of ($M_{\text{w}}/M_{\text{n}} = 7.3$). Further parameters are $T_{\text{m}}^0 = 483 \,\text{K}$, $Q^* = 6270 \,\text{J mol}^{-1}$ and $K_{\text{g}} = 5.50 \times 10^5 \,\text{K}^2$ [1]. The automaton cell size amounts to $\lambda_{\text{m}} = 1 \,\mu\text{m}$.

2.8. Nucleation criteria

The initial number of nuclei was taken from experimental data on iPP provided by the group of Fulchiron [1, 21]. The nucleation data for isothermal *quiescent* crystallization were obtained by counting the activated nuclei by numbering them on pictures taken through an optical microscope in conjunction with a Linkam heating stage. When the sample was exposed to weak shear flows, the nucleation data had to be calculated from the experiments by using a kinetic model described in [1]. In this approach, the additional number of activated nuclei under the effect of flow is related to the first normal stress difference. The model predicts a continuous increase in the number of activated nuclei as a function of the shearing time. The density of the nuclei saturates at a plateau, the exact value of which is determined by the magnitude of the shear imposed. When applied to a case where shear was imposed, the current simulations used as initial nucleation density a value obtained for a time of 100 s after the onset of shear. After this time period, the nucleation density reaches a plateau value. Direct experimental data on the increase in the nucleation density under the influence of shear were rarely reported, owing to the experimental difficulties associated with this problem (see [33]).

3. Simulation results and discussion

3.1. Kinetics and spherulite structure for quiescent conditions

This section presents three-dimensional cellular automaton simulation results of spherulite growth under quiescent conditions. Each simulation is based on 10 million lattice cells.

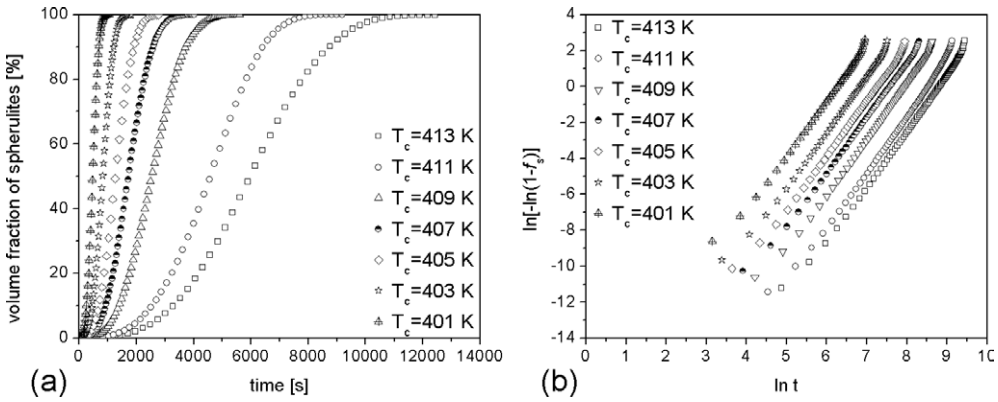

Figure 1. Simulation results: (*a*) simulated kinetics of the volume fraction occupied by spherulites (f_s); (*b*) Avrami analysis for different crystallization temperatures between 401 and 413 K under isothermal quiescent conditions.

The use of experimental input data for the Hoffman–Lauritzen scaling procedure outlined earlier allows us to compare the predictions directly with experimental observations in terms of the crystallization time, kinetic exponents, spherulite topology and resulting spherulite size distributions.

Figure 1 shows the kinetics for simulations over the range of the crystallization temperature T_c between 401 and 413 K under isothermal quiescent conditions. The calculations were conducted with experimental data for the nucleation density [1, 21] for each of the simulated crystallization temperatures. Figure 1(*a*) shows the volume fractions occupied by spherulites as a function of the isothermal heat treatment time. It is important to note in this context, that the depicted *spherulite* volume fraction must not be confused with the *crystalline* volume fraction, since the spherulites are two-phase aggregates consisting of heavily branched crystalline lamellae with amorphous chains between them. The kinetic anisotropy which is principally inherent in such structures at the nanoscopic scale in terms of secondary nucleation events on the lateral lamellae surfaces and of in-plane lamella growth [34, 35] is homogenized at the mesoscopic scale, where the growing spherulites typically behave as isotropic spheres.

The half crystallization times (figure 2) and the Avrami exponents which were obtained from the cellular automaton data via fitting (figure 1(*b*), $n = 3.0 \pm 0.1\%$) are in excellent agreement with analytical three-dimensional results, and with the data reported from experiments for instantaneous nucleation in polypropylene under isothermal quiescent crystallization conditions [1, 36]. The kinetics is expected to decrease with increasing T_c because the nucleation density decreases at higher T_c [1]. This tendency is reproduced well in figure 1(*a*), i.e. the curves for higher values of T_c are shifted towards longer times. The half crystallization times over the entire range of T_c inspected (figure 2) also show good agreement with those determined experimentally by the use of different experimental techniques such as DSC, rheometry and optical microscopy [1].

The scatter in the data for the spherulite volumes at large times (figure 1(*b*)) (particularly above 99% spherulite volume), is due to the fact that the simulated transformation from the melt to the spherulite state performed by the last cell switches becomes increasingly discrete owing to the changing ratio between the final non-transformed volume and the switched cells. This is coherent with the fact that during the final growth stage, mutual impingement of expanding spherulites affects their further isotropic growth [37]. The relevance of the data predicted for the *final* stages of the transformation is, therefore, somewhat overemphasized and should be treated

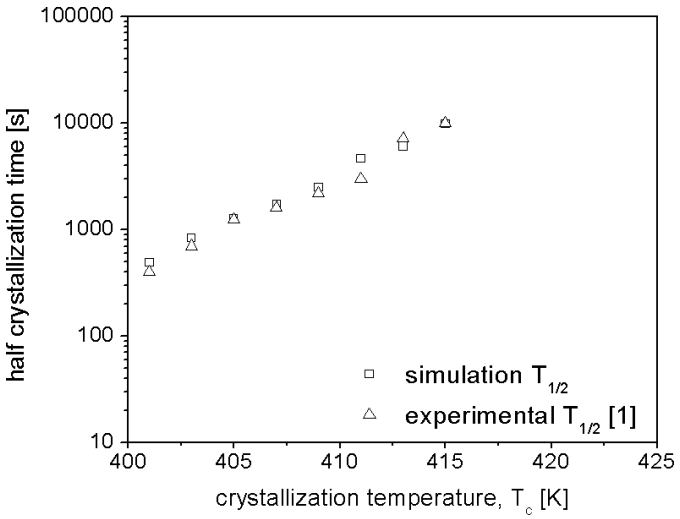

Figure 2. Comparison between experimentally obtained [1] and simulated data of the half crystallization times for various crystallization temperatures under isothermal quiescent conditions. The data reveal excellent agreement.

with some skepticism, for instance, when analysing simulated kinetic exponents at the very end of the transformation. The simulation results presented were obtained from three simulation runs which were conducted for each set of starting conditions, in order to capture statistical effects arising from the Monte Carlo integration scheme. The results substantiate the statistical fluctuations in the simulation procedure being insignificant.

Figure 3 shows the effect of the crystallization temperature, T_c, on the final microstructure developed under isothermal quiescent conditions. The final size of the spherulites is increased as a result of the increase in T_c. This effect can be fully attributed to the decreased nucleation density at the higher crystallization temperatures. Figure 4 presents the corresponding Cahn–Hagel diagrams for the simulations presented in figures 1–3. Cahn–Hagel diagrams quantify the ratio of the total interfacial area of all spherulites with the residual amorphous matrix (melt), and the sample volume as a function of the spherulitic volume fraction. It can be used to study the system homogeneity which is a relevant aspect associated with discrete models. For a statistical Avrami-type situation at different values for T_c with different, nucleation densities, the Cahn–Hagel curve assumes a maximum at 50% spherulite growth, which is well fulfilled for the present simulations.

Figure 5 shows the resulting spherulite size distributions in terms of the spherulite volumes over the range of T_c investigated. The diagrams use a logarithmic axis for the spherulite size classes and a normalized axis for the spherulite frequencies (number of spherulites in each size class divided by the *total* number of spherulites). This type of presentation allows one to compare the different simulation results over a wide spectrum of boundary conditions. The results were fitted by using a logarithmic normal distribution (solid line in each diagram) which is typically fulfilled for Avrami-type growth processes with site-saturated nucleation conditions. The comparison shows that the simulations indeed reproduce the statistical topological behaviour of Avrami processes very well. The data document very well the (obvious) gradual shift of the final spherulite size distributions from conditions with a large number of initial nuclei (figure 5(a), $T_c = 401$ K, small average spherulite size) to conditions with a small number of initial nuclei (figure 5(f), $T_c = 413$ K, large average spherulite size).

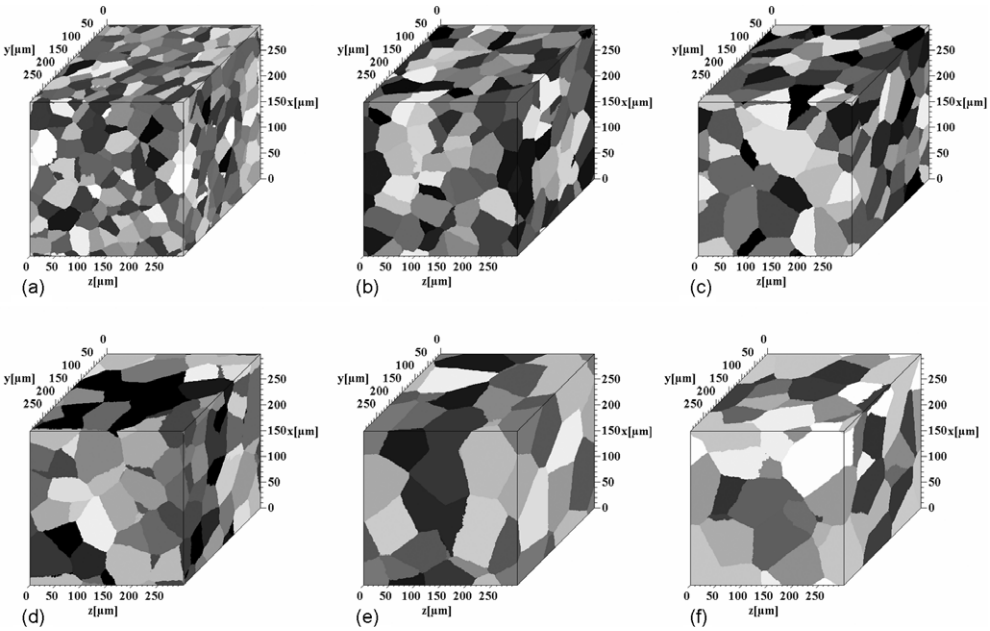

Figure 3. Simulated spherulite microstructures for different isothermal crystallization temperatures, T_c, using different experimental values of the nucleation density under quiescent conditions. The various grey scales identify the different spherulites. (*a*) $T_c = 401$ K, (*b*) $T_c = 403$ K, (*c*) $T_c = 405$ K, (*d*) $T_c = 407$ K, (*e*) $T_c = 411$ K and (*f*) $T_c = 413$ K.

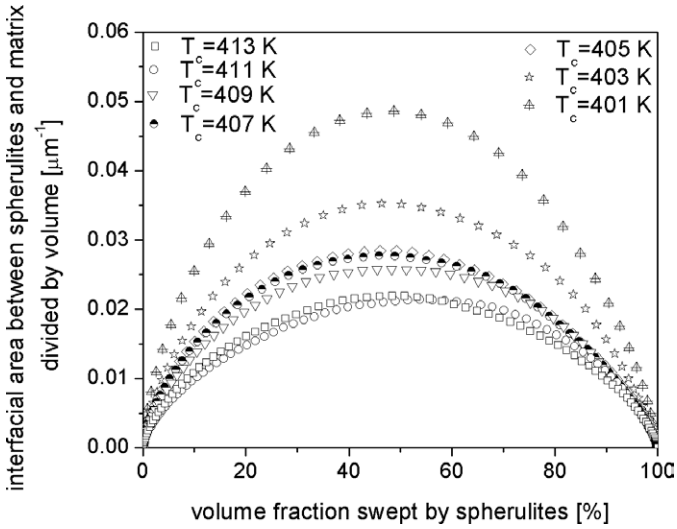

Figure 4. Cahn–Hagel diagram for the simulations presented in figures 1–3. The diagram presents the total interfacial area between the spherulitic material and the residual melt, divided by the sample volume as a function of the spherulitic volume fraction.

3.2. Kinetics and spherulite structure under weakly sheared conditions

The simulations were also conducted for crystallization processes under weak flow conditions placing particular attention on the influence of the shear rate, $\dot{\gamma}$, and shearing time, t_s. As a rule,

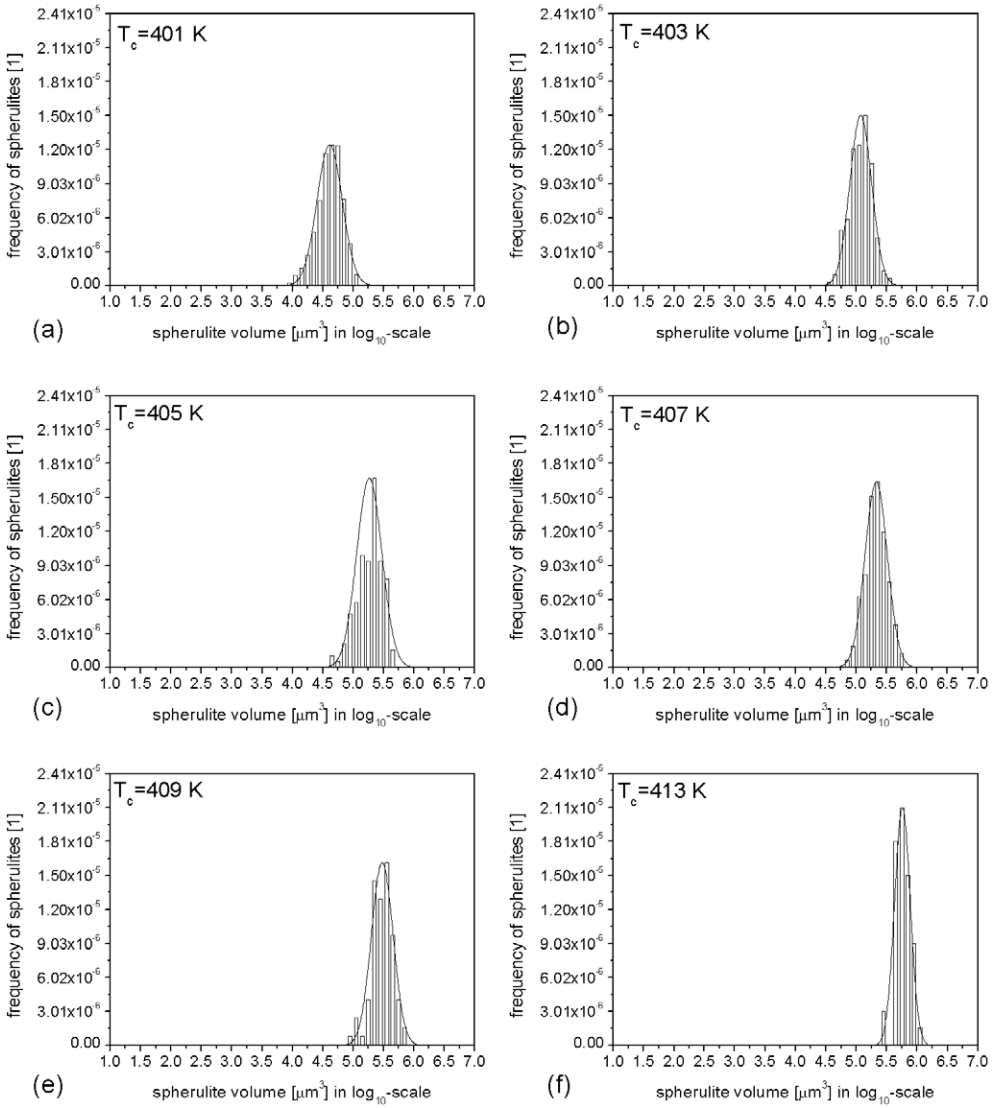

Figure 5. Simulated spherulite size distributions in terms of the spherulite volumes obtained from quiescent crystallization for different isothermal crystallization temperatures. The data are presented by using a logarithmic axis for the spherulite size classes, and a normalized axis for the spherulite frequencies (number of spherulites in each size class divided by the *total* number of spherulites). The lines represent curve fits by use of a logarithmic normal distribution.

crystallization processes under shear flows are generally accelerated compared to quiescent conditions, i.e. the crystallization times drop significantly when the melt is sheared. The most important effect in that context comes from an increasing number of nuclei under shear [1]. The nucleation density data for such situations can be calculated by using a kinetic model as suggested in [1]. We used the data after 100 s of imposed shear as input data for studying the effect of both, the shear rate and the shearing time in the simulations. The micrographs which document the experiments of Fulchiron and Koscher [1] suggest that at higher shear rates and

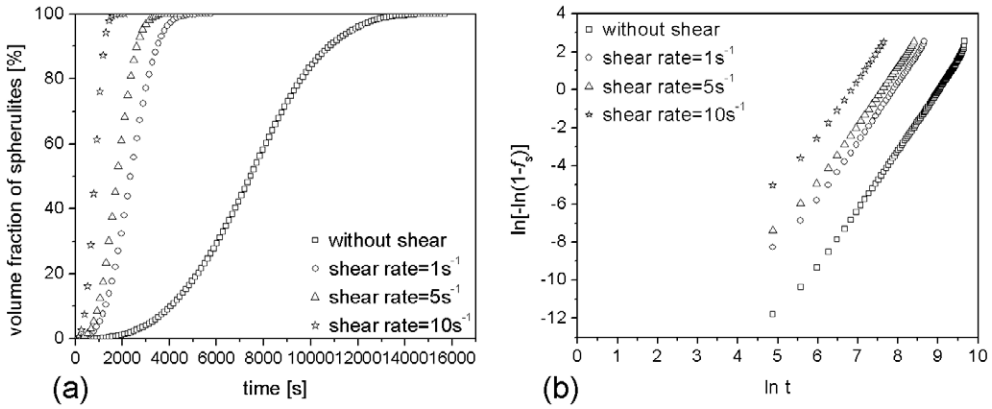

Figure 6. Simulation results: (*a*) simulated kinetics of the volume fraction occupied by spherulites (f_s); (*b*) Avrami analysis under isothermal crystallization conditions (crystallization temperature $T_c = 413$ K) investigated under a constant shearing time, $t_s = 10$ s, for various shear conditions.

shearing times, a different type of nuclei (row nuclei) can be observed before the formation of independent nuclei at larger times. Fulchiron has reported that no substantial effect of the shear on the *growth rates* of the spherulites was observed.

3.2.1. Effect of the shear rate. The effect of an increase in the shear rate imposed on a melt for a constant shearing time ($t_s = 10$ s) under otherwise isothermal crystallization conditions, $T_c = 413$ K, is significant, both with respect to the resulting spherulite morphology and the overall crystallization kinetics. Since the literature suggests that the actual growth rate of a spherulite is not greatly affected by the melt flow [1], we did not alter the growth scaling law (see chapter 2) for the current simulations. Instead, we used the corresponding nucleation density data corrected for shear as outlined earlier. The Avrami analysis is given in figure 6. As expected, it reveals an increase in the kinetics for growing shear rates. This effect may be attributed to the increase in the number of available nuclei. The Avrami constant amounts, in all cases, to $n = 3.0 \pm 0.1\%$ which is in excellent accord with the literature data [36] under flow for iPP under isothermal crystallization conditions. This observation (i.e. $n \approx 3.0$) also underlines the fact that the growth rate is affected only by the number of available nuclei and obviously not much by weak shears. Figure 7 shows the resulting microstructures for some selected cases.

Figure 8 shows the resulting simulated spherulite size distributions in terms of the spherulite volumes for the different shear rates. The simulated size distributions reveal the decrease in the average spherulite volumes with increasing shear rates due to the increase in the nucleation density.

3.2.2. Effect of shearing time. We also studied the effect of the shearing time at a constant shear rate of 5 s^{-1} on the crystallization kinetics, and microstructure by means of the cellular automaton method. The Avrami analysis (figure 9) reveals an increase in the crystallization rate. Figure 10 shows the corresponding microstructure, revealing the reduced final sizes of the spherulites as a function of the increased shearing times.

Figure 11 shows the resulting simulated spherulite size distributions in terms of the spherulite volumes for various shearing times. The spherulite volume is decreased due

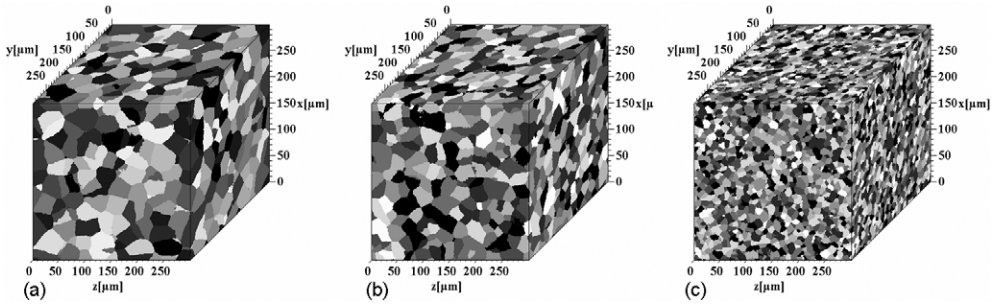

Figure 7. Simulated spherulite microstructures obtained for various shear rates at a constant shearing time of $t_s = 10$ s under isothermal conditions ($T_c = 413$ K) for different values of the nucleation density. The various grey scales identify the different spherulites. (*a*) Shear rate $= 1\ s^{-1}$, (*b*) shear rate $= 5\ s^{-1}$ and (*c*) shear rate $= 10\ s^{-1}$.

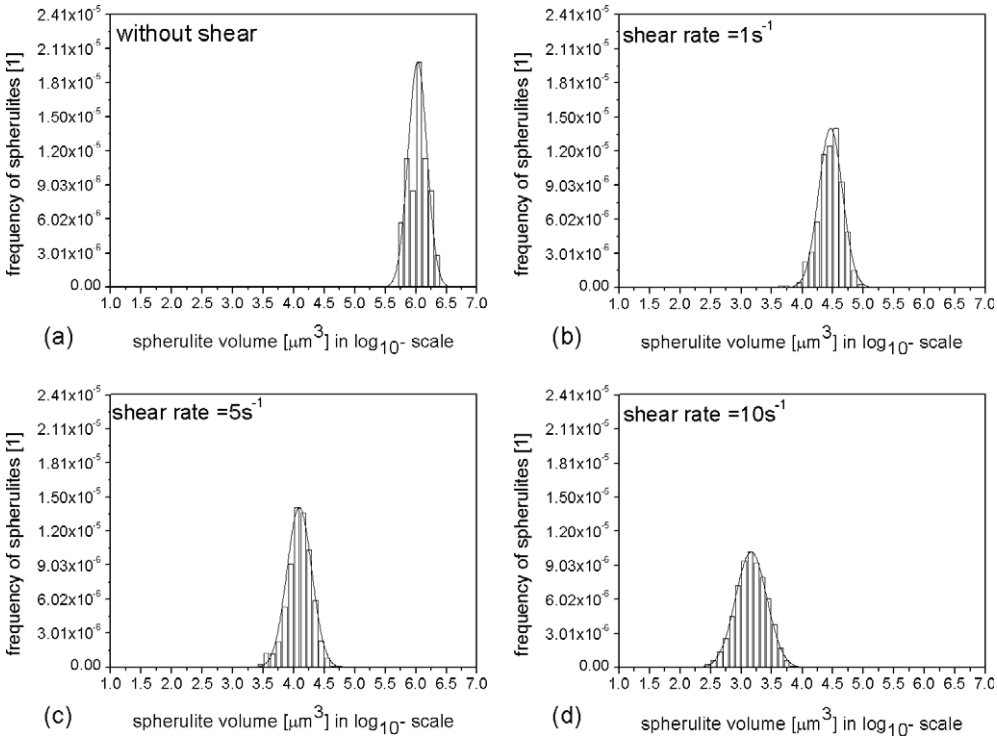

Figure 8. (*a*)–(*d*) Simulated spherulite size distributions in terms of the spherulite volumes under an imposed shear flow showing the effect of different shear rates for constant shearing times ($t_s = 10$ s) at an isothermal crystallization temperature of $T_c = 413$ K. The data are presented by using a logarithmic axis for the spherulite size classes and a normalized axis for the spherulite frequencies (number of spherulites in each size class divided by the *total* number of spherulites). The lines represent curve fits by the use of a logarithmic normal distribution.

to an increase in the nucleation density with increasing shearing times at a constant shear rate of $5\ s^{-1}$.

The simulation results substantiate the cellular automaton model being capable of predicting the correct trends for both, the influence of the shear rate (figure 12(*a*)) and for the

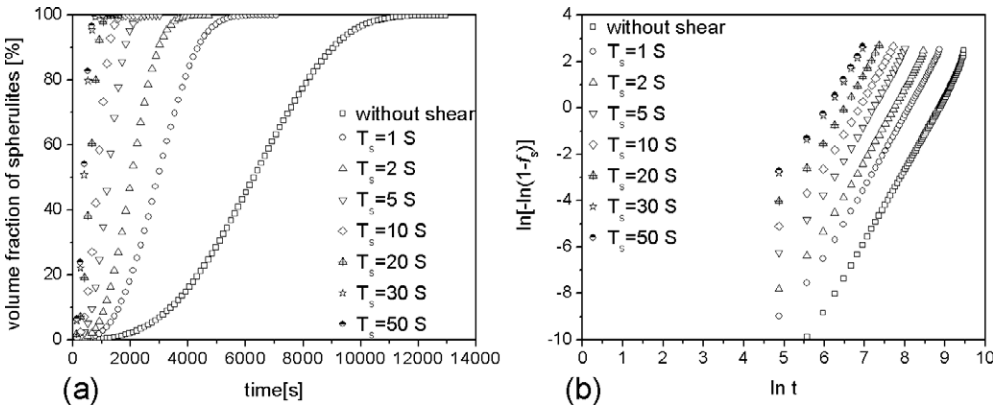

Figure 9. Simulation results: (*a*) simulated kinetics of the volume fraction occupied by spherulites (f_s); (*b*) Avrami analysis under isothermal crystallization conditions at a temperature of $T_c = 413$ K investigated under a constant shear rate of = 5 s^{-1} at various shearing times, t_s.

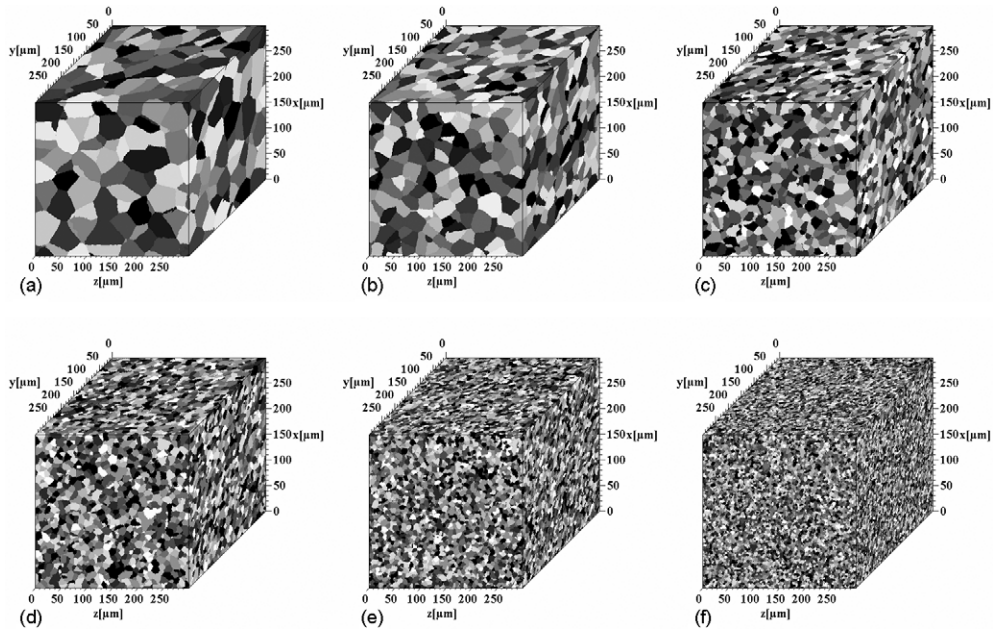

Figure 10. Simulated spherulite microstructures after various shearing times, t_s, at a constant shear rate of 5 s^{-1} under isothermal conditions ($T_c = 413$ K) for different values of the nucleation density [18]. The various grey scales identify the different spherulites. (*a*) $t_s = 1$ s, (*b*) $t_s = 2$ s, (*c*) $t_s = 5$ s, (*d*) $t_s = 10$ s, (*e*) $t_s = 20$ s and (*f*) $t_s = 30$ s.

shearing time (figure 12(*b*)) on the overall crystallization kinetics compared with experimental data from the literature [1]. The figures show excellent agreement for the effect of the shear rate (figure 12(*a*)), although deviations occur for higher shearing times (figure 12(*b*)).

As mentioned earlier, the kinetic model used by Fulchiron and Koscher [1] for the calculation of the increase in the nucleation density under shear flows, suggests an increase in the nucleation density as a function of time, which could result in an over-estimation of the

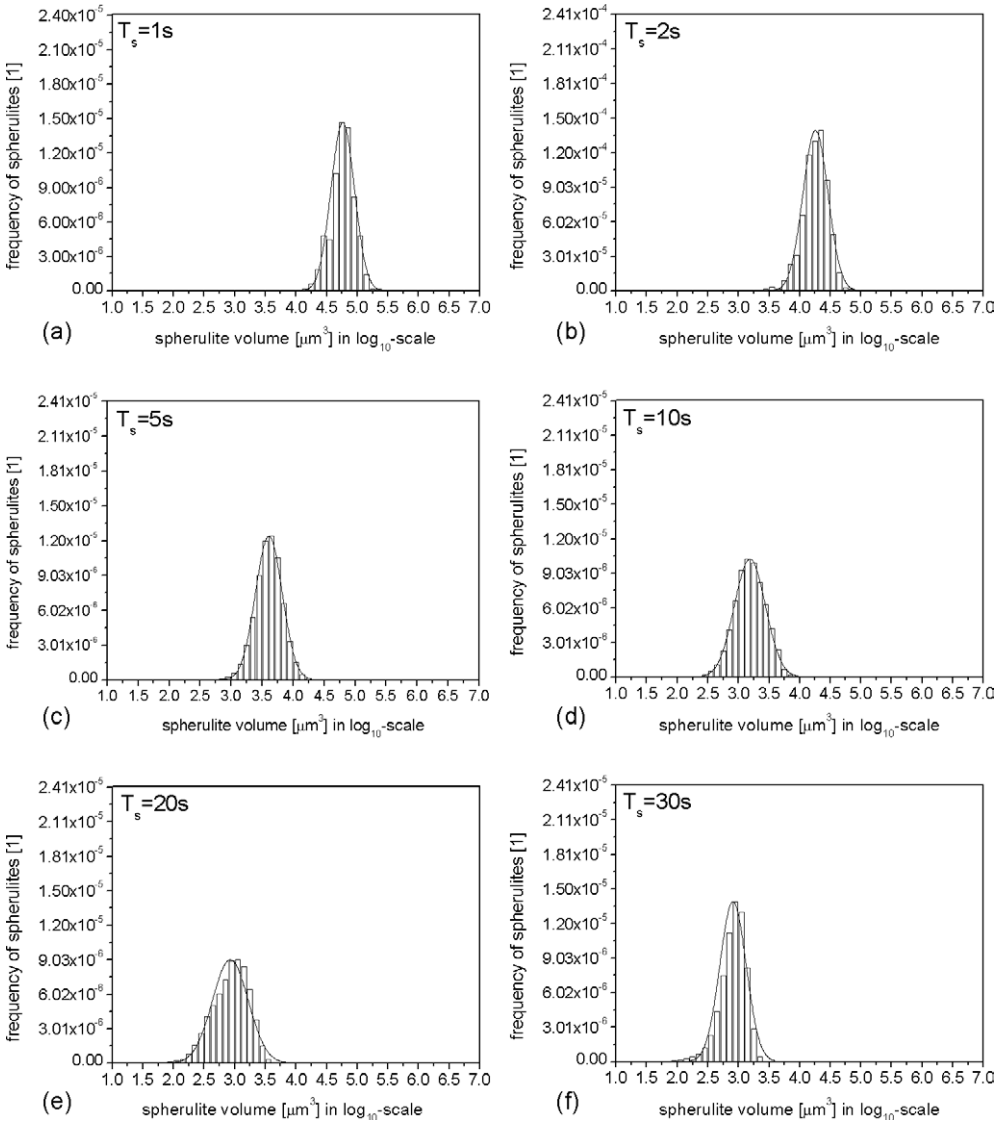

Figure 11. (*a*)–(*f*) Simulated spherulite size distributions in terms of the spherulite volumes under weak shear flows showing the effect of varying shearing times under a constant shear rate of $5\,s^{-1}$ at an isothermal crystallization temperature of $T_c = 413\,K$. The data are presented by using a logarithmic axis for the spherulite size classes, and a normalized axis for the spherulite frequencies (number of spherulites in each size class divided by the total number of spherulites). The lines represent curve fits by use of a logarithmic normal distribution.

assumed nucleation density. This effect might explain the fast kinetics predicted by the current automaton simulations when compared with the experimental data (figure 12(*b*)). The observed deviations for larger shearing times suggests that the kinetic model given by Fulchiron and Koscher [1] should be corrected with respect to possible higher order effects. The assumption that the nucleation densities used for the simulations under shear were too large is also supported by the excellent agreement between the experimental results of Fulchiron and Koscher [1] and

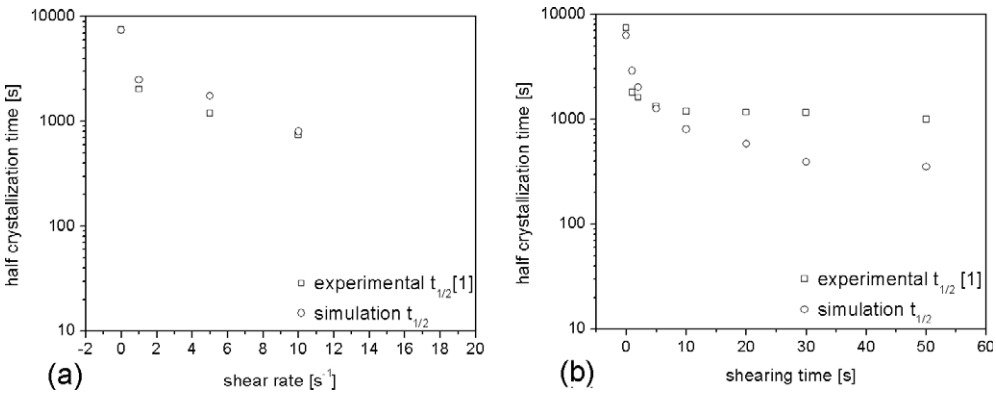

Figure 12. Experimentally observed [1] and simulated half crystallization times versus (*a*) shear rates at a constant shearing time of $t_s = 10$ s; (*b*) shearing times under a constant shear rate $= 5\ s^{-1}$ at an isothermal crystallization temperature of $T_c = 413$ K.

the current simulation results under quiescent conditions, where we used nucleation densities which were directly observed by experiment (figure 2).

Another explanation for the deviations observed (figure 12(*b*)) could be the cumulative effect of the shear rate and of the shearing time on the overall crystallization kinetics as earlier suggested by Devaux *et al* [36]. In their work, the authors introduced a parameter $t_{0,\max}$, to describe the effects of the shear rate and shearing time on the kinetics of crystallization in terms of critical dwell time. Devaux *et al* [36] assumed that if the end of shearing occurs before the critical dwell time $t_{0,\max}$, there is no effect on crystallization. However, if the shear was imposed longer than $t_{0,\max}$, the kinetics was assumed to slow down.

In that context, one may assume that high shear rates entail a drop in $t_{0,\max}$ which, in turn, would slow down the kinetics as discussed earlier. Past the critical dwell period of $t_{0,\max}$, the crystalline growth seems to begin during the period of shearing, i.e. shear-assisted nucleation is not so efficient anymore. The possible coalescence of nuclei, a complex coupling between the variations in density and the shear flow, or, an increased growth rate during flow may also be attributed to the deviations observed [36].

4. Conclusion

A three-dimensional cellular automaton model is critically evaluated with respect to its capability of reproducing spherulite growth in polymers under various boundary conditions. We use polypropylene as a reference material. The automaton is discrete in time and real space. The switching probability of the cells is formulated according to the kinetic theory of Hoffman and Lauritzen. It is scaled by the ratio of the local and the maximum interface energies, the local and maximum occurring Gibbs free energy of transformation, the local and maximum occurring temperature and by the spacing of the lattice points. The use of experimental input data for polypropylene and the subsequent comparison with experimental results allowed us to conduct a *quantitative* validation of the model. The good agreement between simulated and experimental results showed that the model is capable of correctly reproducing the kinetics for instantaneous homogenous nucleation conditions under isothermal quiescent conditions and, even under weak shears. Apart from these basic validation issues, the study aimed at documenting the main advantage of the new model which is its capability of predicting microstructure details which the Avrami-type approximations typically used in

this field, cannot provide. In particular, the new cellular automaton method can tackle the *heterogeneity* of the internal and external boundaries and the starting conditions, which is not possible for Avrami-models. The new automaton approach can, for instance, predict intricate spherulite topologies, spherulite size distributions, kinetic details and crystallographic textures under homogeneous or heterogeneous external or internal boundary conditions. Furthermore, it can be coupled to forming and processing models making use of *local*, rather than only global, boundary conditions.

Acknowledgment

The authors are most grateful to Dr R Fulchiron at the University of Lyon in France for kindly providing the nucleation data for the simulation presented in this paper. Dr R Fulchiron can be reached at Rene.Fulchiron@univ-lyon1.fr.

References

[1] Koscher E and Fulchiron R 2002 *Polymer* **43** 6931
[2] Billon N, Escleine J M and Haudin J M 1989 *Colloid Polym. Sci.* **267** 668
Billon N, Escleine J M and Haudin J M 1989 *Colloid Polym. Sci.* **267** 1064
[3] Billon N, Escleine J M and Haudin J M 1993 *Colloid Polym. Sci.* **271** 343
[4] Piorkowska E J 1995 *Phys. Chem.* **99** 14007
Piorkowska E J 1995 *Phys. Chem.* **99** 14016
Piorkowska E J 1995 *Phys. Chem.* **99** 14024
[5] Mehl A N and Rebenfeld L 1993 *J. Polym. Sci.* B **31** 1677
Mehl A N and Rebenfeld L 1993 *J. Polym. Sci.* B **31** 1687
[6] Nakamura K, Watanabe K, Katayama K and Amano T 1972 *J. Appl. Polym. Sci.* **16** 1077
[7] Ozawa T 1971 *Polymer* **12** 150
[8] Zuidema H, Peters G W M and Meijer H E H 2001 *Macromolecules Theory Simul.* **10** 447
[9] Eder G and Janeschitz-Kriegl H 1997 *Processing of Polymers* vol 18, ed H E H Meijer (Ser. ed R W Cahn *et al*) (New York: VCH) chapter 5, p 269
[10] Eder G, Janeschitz-Kriegl H and Krobath G 1989 *Prog. Colloid Polym. Sci.* **80** 1
[11] Hieber C A 1995 *Polymer* **36** 1455
[12] Raabe D 2004 *Acta Mater.* **52** 2653
[13] Michaeli W, Hoffmann S, Cramer A, Dilthey U, Brandenburg A and Kretschmer M 2003 *Adv. Eng. Mater.* **5** 133
[14] Raabe D and Chen N 2004 *REX&GG 2004: Proc. 2nd Joint Int. Conf. on Recrystallization and Grain Growth (Annecy, France)* ed B Bacroix *et al* (Zurich, Switzerland: Trans Tech Publications) *Mater. Sci. Forum* **467–470** 551
[15] von Neumann J 1987 The general and logical theory of automata *Papers of John von Neumann on Computing and Computer Theory* (*Charles Babbage Institute Reprint Series for the History of Computing* vol 12) ed W Aspray and A Burks (Cambridge, MA: MIT Press)
[16] Raabe D 2002 *Annu. Rev. Mater. Res.* **32** 53
[17] Raabe D 1999 *Phil. Mag.* A **79** 2339
[18] Raabe D and Becker R 2000 *Modelling Simul. Mater. Sci. Eng.* **8** 445
[19] Raabe D 1998 *Computational Materials Science* (Weinheim: Wiley-VCH)
[20] Raabe D, Roters F, Barlat F and Chen L-Q (ed) 2004 *Continuum Scale Simulation of Engineering Materials—Fundamentals—Microstructures—Process Applications* (Weinheim: Wiley-VCH)
[21] Fulchiron R 2004 private communication
[22] Lauritzen J I and Hoffman J D 1960 *J. Res. Natl Bur. Stand.* **64** 73
[23] Hoffman J D, Davis G T and Lauritzen J I 1976 *Treatise of Solid State Chemistry* vol 3, ed N B Hanney (New York: Plenum) chapter 7, p 497
[24] Hoffman J D and Miller R L 1997 *Polymer* **38** 3151
[25] Keller A 1957 *Phil. Mag.* **2** 1171
[26] Toda A and Keller A 1993 *Colloid Polym. Sci.* **271** 328
[27] Turnbull D and Fisher J C 1949 *J. Chem. Phys.* **17** 71

[28] Keller A 1968 *Rep. Prog. Phys.* **31** 623
[29] Snyder C R, Marand H and Mansfield M L 1996 *Macromolecules* **29** 7508
[30] Snyder C R and Marand H 1997 *Macromolecules* **30** 2759
[31] Long Y, Shanks R A and Stachurki Z H 1995 *Prog. Polym. Sci.* **20** 651
[32] Point J J and Janimak J J 1993 *J. Cryst. Growth* **131** 501
[33] Moitzi J and Skalicky P 1993 *Polymer* **34** 3168
[34] Hobbs J K, Humphris A D L and Miles M J 2001 *Macromolecules* **34** 5508
[35] Hobbs J K, McMaster T J, Miles M J and Barham P J 2001 *Polymer* **39** 2437
[36] Devaux N, Monasse B, Haudin J M, Moldenares P and Vermant J 2004 *Rheo Acta* **43** 210
[37] Eder G 1997 Fundamentals of structure formation in crystallizing polymers *Macromolecular Design of Polymeric Materials* ed K Hatada *et al* (New York: Dekker) p 761